arXiv:1701.01624v3 [cond-mat.quant-gas] 4 Apr 2017

# Phase Diagram of Bosons in a 2D Optical Lattice with infinite-range Cavity-mediated Interactions

T. Flottat,[1] L. de Forges de Parny,[2,3] F. Hébert,[4,*] V. G. Rousseau,[5] and G. G. Batrouni[4,6,7]

[1] *Université Côte d'Azur, CNRS, INLN, Valbonne, 06560, France*
[2] *Laboratoire de Physique, CNRS UMR 5672, École Normale Supérieure de Lyon, Université de Lyon, 46 Allée d'Italie, Lyon, F-69364, France*
[3] *Physikalisches Institut, Albert-Ludwigs Universität Freiburg, Hermann-Herder Straße 3, D-79104, Freiburg, Germany*
[4] *Université Côte d'Azur, CNRS, INLN, France*
[5] *Physics Department, Loyola University New Orleans, 6363 Saint Charles Ave., LA 70118, USA*
[6] *MajuLab, CNRS-UNS-NUS-NTU International Joint Research Unit UMI 3654, Singapore*
[7] *Centre for Quantum Technologies, National University of Singapore; 2 Science Drive 3 Singapore 117542*

High-finesse optical cavity allows the establishment of long-range interactions between bosons in an optical lattice when most cold atoms experiments are restricted to short-range interactions. Supersolid phases have recently been experimentally observed in such systems. Using both exact quantum Monte Carlo simulations and Gutzwiller approximation, we study the ground state phase diagrams of a two-dimensional Bose-Hubbard model with infinite-range interactions which describes such experiments. In addition to superfluid and insulating Mott phases, the infinite-range checkerboard interactions introduce charge density waves and supersolid phases. We study here the system at various particle densities, elucidate the nature of the phases and quantum phase transitions, and discuss the stability of the phases with respect to phase separation. In particular we confirm the existence and stability of a supersolid phase detected experimentally.

PACS numbers: 03.75.Hh, 05.30.Jp, 64.60.F-

## I. INTRODUCTION

In the past fifteen years, cold atoms and Bose Einstein condensates have proven invaluable tools to study the physics of interacting quantum systems[1]. Optical lattices[1,2] and Feshbach resonances[3] have been used to drive these systems into strongly interacting regimes. Recently, it has been shown that coupling between cold atoms and an electromagnetic field, for example by putting a condensate in a cavity, leads to interesting collective phases of light and matter[4]. For example, the Dicke transition[5], superradiant Mott phases[6], self structuration of atoms and light[7], and crystallization[8] have been observed in such systems. Many theoretical predictions have also been made such as the possibility to observe Bose glasses[9], localization[10], or synchronization of quantum dipoles[11].

Here we are especially interested in a recent experiment by the ETH-Zurich group[12] where a cloud of cold atoms is placed in an optical lattice and inside an optical cavity. The field of the cavity mediates an effective infinite range interaction between the atoms which favours a density difference between neighbouring sites of the optical lattice. This experiment attracted a strong interest as it provides one of the first observations of the elusive supersolid phase[13,14]. This exotic phase is characterized by both long range phase coherence and spatial ordering, i.e. simultaneous diagonal and off-diagonal long range orders. In a recent experiment, the same group observed a supersolid phase with a symmetry breaking of a continuous space invariance[15].

The experimental system is well described by a conventional Bose-Hubbard model with an additional infinite range interaction[12], which takes into account the effect of the cavity field. This model and similar ones have been mostly studied within the (static and dynamic) mean-field theory[16–20]; only one study has employed an exact quantum Monte Carlo method in the hard-core limit[21]. In the current state of the literature, exact studies in the strong (but finite) interacting regime are still missing.

In this work, we use exact quantum Monte Carlo simulations to determine the phase diagram of this model for several particle fillings, and elucidate the nature of the observed quantum phase transitions. We also compare our results with mean-field results, obtained with an approach based on the Gutzwiller ansatz and classical Monte Carlo simulations[22,23].

The paper is organized as follows: The Hamiltonian and the methods used are presented in Sec. II. Section III is devoted to the discussion of the mean field phase diagrams whereas the exact ground-state phase diagrams, obtained by using quantum Monte Carlo simulations, are discussed in Sec. IV. Finally, conclusions and outlook are provided in Sec. V.

## II. HAMILTONIAN AND METHODS

### A. Bose-Hubbard model with infinite-range checkerboard interactions

We consider spinless bosons in a two-dimensional square optical lattice inside a high-finesse optical cavity. The particles can hop between nearest neighbouring

sites of the lattice and interact repulsively on site. An additional effect due to the external cavity field generates an effective infinite-range interaction between particles[12]. Integrating out the effect of the field, the system is then shown to be governed by a Bose-Hubbard model with Hamiltonian[12]:

$$\hat{\mathcal{H}} = -t \sum_{\langle \mathbf{r},\mathbf{s} \rangle} \left( b_{\mathbf{r}}^{\dagger} b_{\mathbf{s}} + \text{H.c.} \right) + U_s \sum_{\mathbf{r} \in e,o} \frac{n_{\mathbf{r}} \left( n_{\mathbf{r}} - 1 \right)}{2} - \frac{U_l}{L^2} \left( \sum_{\mathbf{r} \in e} n_{\mathbf{r}} - \sum_{\mathbf{r} \in o} n_{\mathbf{r}} \right)^2 . \quad (1)$$

The bosonic operator $b_{\mathbf{r}}^{\dagger}$ ($b_{\mathbf{r}}$) creates (annihilates) an atom at site $\mathbf{r}$ and $n_{\mathbf{r}} = b_{\mathbf{r}}^{\dagger} b_{\mathbf{r}}$ is the corresponding number operator. The indices $e$ and $o$ denote respectively even and odd lattice sites. The first term of the Hamiltonian is the kinetic term describing tunnelling with amplitude $t$ between nearest neighbour sites $\mathbf{r}$ and $\mathbf{s}$ defined on a square lattice of $L \times L$ sites with periodic boundary conditions. The second term represents the on-site repulsive interactions between the atoms with strength $U_s > 0$. The third term describes the infinite-range interaction with amplitude $U_l > 0$ and favours imbalanced populations between even and odd sites. $\mu$ will denote the chemical potential for simulations performed in the grand canonical ensemble (GCE).

The Hamiltonian has a $U(1) \times \mathbb{Z}_2$ symmetry, associated with the mass conservation ($U(1)$ symmetry), times the Ising $\mathbb{Z}_2$ symmetry between the even and odd checkerboard sublattices.

### B. Methods

The approximate Gutzwiller Monte Carlo (GMC)[22,23] approach is a numerical method built on the combination of both the Gutzwiller ansatz and the classical Monte Carlo method with Metropolis algorithm[24]. This results in a semi-classical lattice field theory which preserves the $U(1)$ symmetry, which is an advantage compared to some of the mean-field approaches conventionally used. This method also allows the reconstruction of correlation functions on a finite lattice cluster. The Gutzwiller mean-field state takes the form

$$|\Psi(\mathbf{f})\rangle = \bigotimes_{\mathbf{r}=1}^{L^2} |\psi_{\mathbf{r}}\rangle = \bigotimes_{\mathbf{r}=1}^{L^2} \left( \sum_{n_{\mathbf{r}}=0}^{n_{\max}} f_{n_{\mathbf{r}}}^{(\mathbf{r})} |n_{\mathbf{r}}\rangle \right) , \quad (2)$$

where $|n_{\mathbf{r}}\rangle$ is the state with $n_{\mathbf{r}}$ particles on site $\mathbf{r}$ and where we introduced a cut-off $n_{\max}$ on the number of particles per site. The ensemble $\mathbf{f} = \{f_{n_{\mathbf{r}}}^{(\mathbf{r})}\}$ of the complex $f_{n_{\mathbf{r}}}^{(\mathbf{r})}$ coefficients is then sampled with the Monte Carlo method[22,23] which is especially useful at finite temperature but can also be used in the low temperature regime.

The Hamiltonian is also simulated by using the stochastic Green function algorithm (SGF)[25,26], an exact quantum Monte Carlo (QMC) technique that allows simulations in the canonical (CE) or grand canonical (GCE) ensembles of the system at finite temperatures, as well as measurements of many-particle Green functions.

We treat $L \times L$ lattices with sizes up to $L = 14$ and fix $t = 1$ to set the energy scale. Large enough inverse temperatures allow to eliminate thermal effects from the QMC and GMC results (we used inverse temperatures $\beta t = 2L$ for the QMC simulations and up to $\beta t = 10^4$ for the GMC simulations).

In particular we focus mainly on simulations at fixed density $\rho = \sum_{\mathbf{r}} \langle n_{\mathbf{r}} \rangle / L^2$. $N = \rho L^2$ is the total number of particles. The phase coherence is captured by the one body Green function,

$$G(\mathbf{R}) = \frac{1}{2L^2} \sum_{\mathbf{r}} \langle b_{\mathbf{r}}^{\dagger} b_{\mathbf{r}+\mathbf{R}} + \text{H.c.} \rangle \quad (3)$$

and its Fourier transform $n(\mathbf{k})$ is the density of particles occupying the wave vector $\mathbf{k}$. The condensate fraction, i.e. the fraction of particles occupying the $\mathbf{k} = 0$ mode, is given by $n(\mathbf{k} = 0) = \sum_{\mathbf{R}} G(\mathbf{R})/N$. We also calculate the superfluid density $\rho_s$ given, in the QMC algorithm, by fluctuations of the winding number[27] $W$, $\rho_s = \langle W^2 \rangle / (4t\beta)$. Finally, we also calculate the density-density correlation

$$D(\mathbf{R}) = \frac{1}{L^2} \sum_{\mathbf{r}} \langle n_{\mathbf{r}} n_{\mathbf{r}+\mathbf{R}} \rangle \quad (4)$$

and its Fourier transform, the structure factor $S(\mathbf{k}) = \sum_{\mathbf{R}} e^{i\mathbf{k}.\mathbf{R}} D(\mathbf{R})/L^2$. We particularly focus on $S(\pi, \pi)$ as we expect checkerboard phases to appear.

## III. GUTZWILLER PHASE DIAGRAMS

Since competing terms are involved in the Hamiltonian, Eq. (1), we expect four different phases at zero temperature. For $U_l = 0$, i.e. the standard Bose-Hubbard model, it is well known that the competition between the kinetic and interacting terms leads to two phases. Most of the phase diagram consists of a Bose condensed (BEC) superfluid phase (SF) which exhibits phase coherence indicated by $n(\mathbf{k} = 0) \neq 0$ and $\rho_s \neq 0$. For integer particle densities, $\rho$, and strong repulsion, $U_s$, there are also Mott insulating (MI) phases with $n(\mathbf{k} = 0) = 0$ and $\rho_s = 0$. Adding the checkerboard interaction $U_l \neq 0$ offers the possibility to stabilize spatial ordering, i.e. oscillations in the density signalled by $S(\pi, \pi) \neq 0$. In addition to the SF and MI phases – for which $S(\pi, \pi) = 0$ as the populations are balanced in these phases – there is, therefore, the possibility of two other phases: a charge density wave (CDW) solid with vanishing coherence (for integer or half-integer densities) and a supersolid (SS) phase exhibiting both spatial ordering $S(\pi, \pi) \neq 0$ and phase coherence. In Fig. 1, we show $\rho$, $n(\mathbf{k} = 0)$, and $S(\pi, \pi)$ as functions of the chemical potential, $\mu$. We observe the four previously mentioned phases. The truncation $n_{\max}$

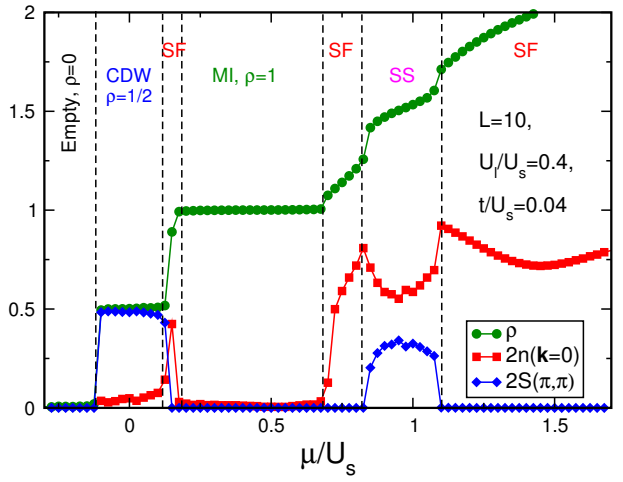


FIG. 1. (Color online) The density, $\rho$, condensate fraction, $n(\mathbf{k}=0)$, and structure factor, $S(\pi,\pi)$, as functions of the chemical potential, $\mu$, obtained with the GMC method at low temperature. We observe four phases: solid with charge density wave (CDW), superfluid (SF), Mott insulator (MI), and supersolid (SS).

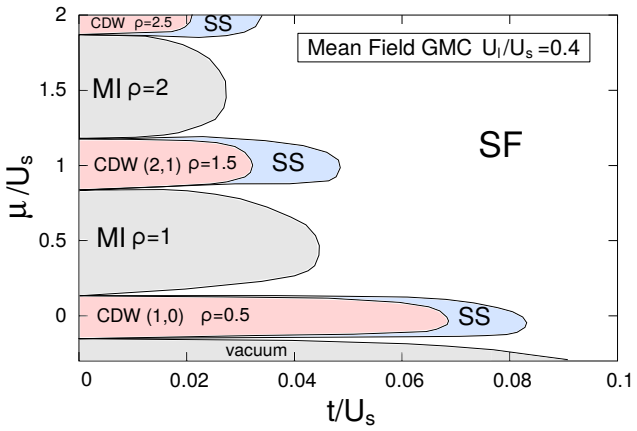


FIG. 2. (Color online) Ground-state mean field phase diagram in the plane $(t/U_s, \mu/U_s)$ obtained with the GMC method for $U_l/U_s = 0.4$. Four phases are observed: superfluid (SF), Mott insulator (MI), charge density wave (CDW) and supersolid (SS) phases.

(up to $n_{\max} = 8$) is chosen large enough for the results not to depend on it and the temperature is chosen low enough to be in the ground state limit.

Using cuts such as Fig. 1, we determined the phase diagrams in the $(t/U_s, \mu/U_s)$ plane for given values of $U_l/U_s$ (see Fig. 2 for $U_l/U_s = 0.4$). The four phases, SF, MI, CDW, and SS, are clearly seen in this phase diagram. In the zero hopping limit $t = 0$, the CDW phases appear between the Mott insulator phases, reducing the energy gap of the MI phases to $\Delta = U_s - U_l$ for $0 < U_l < U_s/2$. At large hopping amplitude $t$ the system is in the SF phase. In the intermediate regime, for moderate hopping, we systematically observe SS phases at the tip of the CDW lobes. Note that this phase diagram is in a good agreement with previous mean field studies[17,18]. The SS-SF phase transition at the tip of the lobes is found to be continuous, as observed in Ref.[17], and not first-order as observed in Ref.[18].

As reported in Refs.[17,18], beyond $U_l = U_s/2$, the nature of the phases change, as phases that show a density modulation are favoured (Fig. 3). The Mott phases are thus replaced with CDW phases. In the small $t$ limit, the Mott phase at $\rho = 1$ is replaced with a phase where, depending on the way the symmetry breaks, even (odd) sites are occupied by 2 bosons while odd (even) sites are empty. This is what we call a CDW (2,0) phase. The CDW phases at half-integer fillings are also affected. For example, the CDW (2,1) phase, i.e. having alternately doubly and singly occupied sites, observed at $\rho = 3/2$ below $U_l/U_s = 1/2$ is replaced with a (3,0) phase. The supersolid region is also much larger as it surrounds completely the CDW lobes for $\rho > 1/2$. The bosons are expected to collapse for $U_l > U_s$ in $t = 0$ limit[18].

We now focus on the phase diagrams in the $(U_s/t, U_l/U_s)$ plane maintaining the density fixed by adjusting the chemical potential. The GMC mean field phase diagrams for densities $\rho = 0.5$, $\rho = 1$, and $\rho = 1.5$ are plotted in Fig. 3. Our results are similar to the phase diagrams of Ref.[17]. We observe that the supersolid phase surrounds CDW phases, which means that it only appears for $U_l/U_s > 1/2$ for integer densities (as $\rho = 1$) while it is present for smaller $U_l$ at half-integer densities. At $\rho = 1/2$, what appears at first sight to be a supersolid phase, where $n(\mathbf{k} = 0)$ and $S(\pi,\pi)$ are both non zero, is not a stable phase but a region of the phase diagram where we observe a phase separation between a superfluid with $\rho < 1/2$ and a supersolid with $\rho > 1/2$ (SF-SS PS region). We will discuss this point later when we will study the stability of the different phases (Sec. IV C).

## IV. QUANTUM MONTE CARLO PHASE DIAGRAMS

Using QMC simulations in the canonical ensemble, we determine exactly the properties of the ground state. We will detail our observations in the following but we first compare the phase diagrams at fixed fillings that we obtained with QMC (Fig. 4) and GMC (Fig. 3). We observe the same features for all phase diagrams, with mostly quantitative differences between the QMC and the GMC predictions. The main difference is that the GMC technique generally overestimates the size of supersolid or phase separation regions. For example, at $\rho = 1/2$ the PS region is difficult to observe below $U_l/U_s = 0.6$ as the transition lines marking the onset of density ordering and the disappearance of condensation appear superimposed in the limits of our simulations (Fig. 4 (a)). For $\rho = 1$, the GMC and QMC phase diagrams are essentially the same but we observe a region

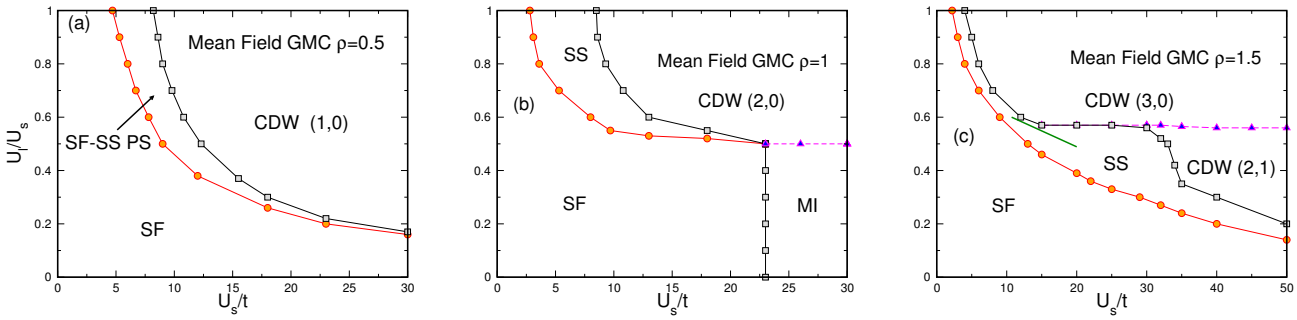


FIG. 3. (Color online) Ground-state mean field phase diagrams obtained with the GMC method for three fillings (a) $\rho = 1/2$, (b) $\rho = 1$ and (c) $\rho = 3/2$. Four stable phases are observed: superfluid (SF), Mott insulator (MI), charge density wave (CDW) and supersolid (SS) phases. The dashed lines indicate first-order transitions, otherwise the transitions are second order. The green line in (c) corresponds to the cut through the SS phase used in Fig. 10 (b). In Sec. IV C, we will discuss the stability of these phases and show that there is a region of phase separation between a superfluid and a supersolid (SF-SS PS) at $\rho = 1/2$ instead of a SS phase.

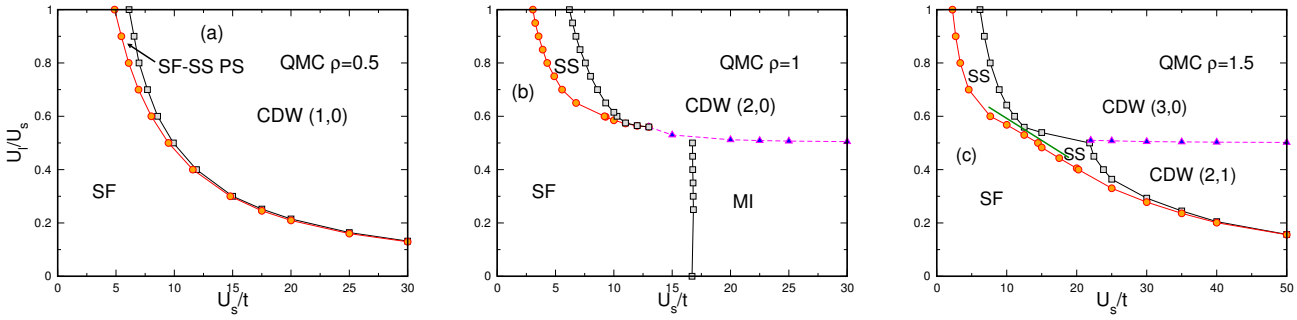


FIG. 4. (Color online) Ground-state phase diagrams obtained with QMC simulations in the canonical ensemble for three fillings (a) $\rho = 1/2$, (b) $\rho = 1$ and (c) $\rho = 3/2$. Four phases are observed: superfluid (SF), Mott insulator (MI), charge density wave (CDW) and supersolid (SS) phases. Dashed lines indicate first-order transition. The black line indicates a 3D XY transition associated with the appearance of a condensed superfluid state. The red line indicates the 3D Ising transition associated with the appearance of density wave. At $\rho = 1$, there is a small region where there is a direct transition between the SF and the CDW (2,0) phases where both the Ising $\mathbb{Z}_2$ and XY $U(1)$ symmetries are broken simultaneously. The green line in (c) corresponds to the cut through the SS phase used in Fig. 10 (a). In Sec. IV C, we will discuss the stability of these phases and show that, while the $\rho = 1$ and $\rho = 3/2$ SS phases are stable, at $\rho = 1/2$ there is, instead, phase separation between a superfluid and a supersolid (SF-SS PS).

where there seems to be a direct transition, without passing via an intermediate SS phase, between the SF and CDW (2,0) region (Fig. 4 (b)). Finally, for $\rho = 3/2$, we observe that the SS phase does not surround the two CDW phases completely but exists for $U_l/U_s \gtrsim 0.3$ (Fig. 4 (c)).

### A. Phases

We first analyse the different properties of the phases using the behaviour of the density-density correlation and Green functions (Fig. 5) in the case where $\rho = 1$. In the BEC or superfluid phase, we observe long range coherence of the phase as evidenced by the saturation at long distance in the Green function $G(\mathbf{R})$ value. The saturation value of $G(\mathbf{R})$ corresponds to the condensate fraction which is not equal to one because of quantum depletion due to the interaction. On the contrary, there is no diagonal order as the density correlation $D(\mathbf{R})$ tends to a plateau with a value equal to the square of the density, $\rho^2 = 1$ in that case. The CDW phase shows strong oscillation around $\rho^2$ at long distance in $D(\mathbf{R})$ while $G(\mathbf{R})$ decays exponentially to zero, which is characteristic of a solid phase. Finally, the supersolid phase shows simultaneously oscillations around plateaux in both $D(\mathbf{R})$ and in $G(\mathbf{R})$, which shows that both diagonal and off-diagonal long range orders are present at the same time. In the Mott phase (not shown here) $G(\mathbf{R})$ decays exponentially to zero while $D(\mathbf{R})$ simply tends to a plateau with a value $\rho^2$.

To confirm the presence of these phases, we performed finite size scaling analyses of the structure factor, $S(\pi, \pi)$, and of the condensate fraction, $n(\mathbf{k} = 0)$. In Fig. 6, we

show that both quantities extrapolate to non zero values in the thermodynamic limit for values of parameters that are chosen in the supersolid region at $\rho = 1$.

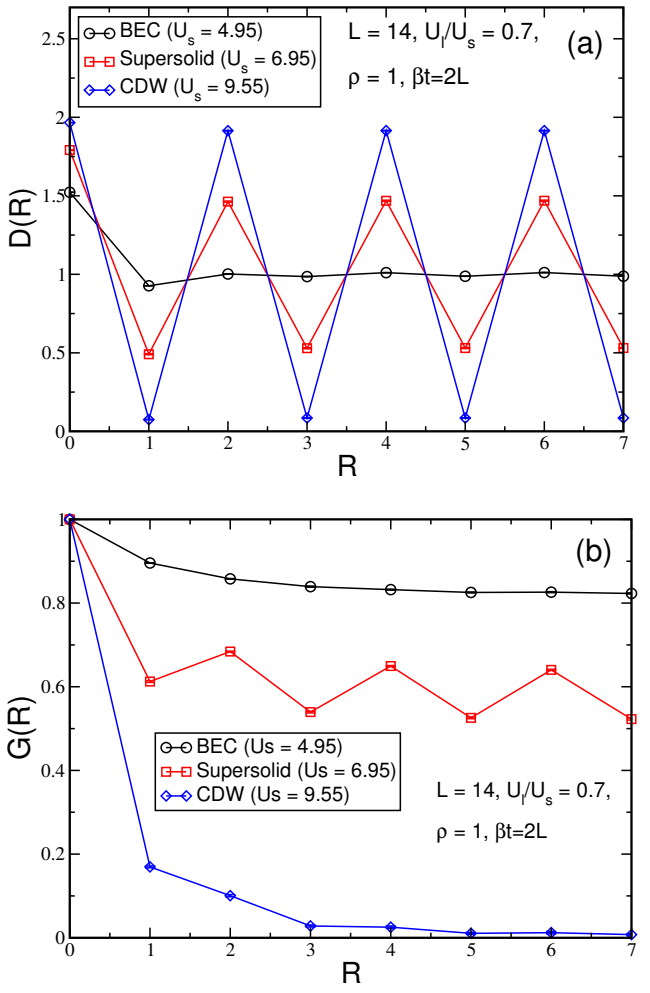


FIG. 5. (Color online) The density-density correlation function $D(R)$ (a) and the Green function $G(R)$ (b) as functions of distance $R$ in different phases at $\rho = 1$ and for a given ratio of interaction $U_l/U_s$. $D$ exhibits long range oscillations in the CDW and supersolid phases. $G$ is non zero at long distances in the supersolid and superfluid phases.

As mentioned earlier, the phases observed change drastically depending on whether $U_l$ is smaller or larger than $U_s/2$. In Fig. 7 (a), we show a cut in the phase diagram, varying $\rho$ for $U_l = 0.45\,U_s$ where we observe all four phases. For small $\rho$, the system is superfluid; for $0.25 \lesssim \rho \lesssim 0.75$, the system shows non zero $S(\pi,\pi)$, which means that it is supersolid (since the condensate is still non zero) except at $\rho = 0.5$ where we find a CDW (1,0) phase. This is somewhat surprising because supersolid phases generally do not appear in large regions of parameter space for $\rho < 1/2$[28]. This effect is due to the infinite range interaction in the system. For $0.75 \lesssim \rho \lesssim 1.25$, $S(\pi,\pi)$ is zero and the system is superfluid except at $\rho = 1$ where it adopts a Mott phase.

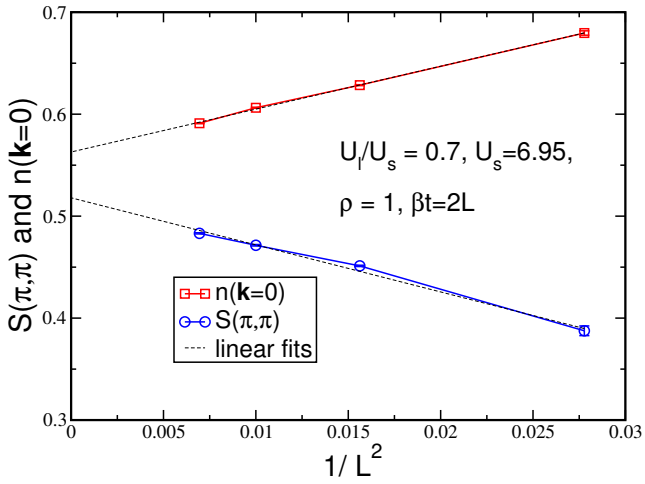


FIG. 6. (Color online) The structure factor $S(\pi,\pi)$ and the condensate fraction $n(\mathbf{k}=0)$ as a function of $1/L^2$ for $\rho = 1$ in the supersolid phase. Both quantities extrapolate to a non zero value for large sizes.

For $1.25 \lesssim \rho < 1.5$, we once again have a supersolid and a CDW (2,1) phase at $\rho = 1.5$. On the contrary for $U_l = 0.8\,U_s$ (Fig. 7(b)), we observe that, for $\rho \geq 1/2$, there are only CDW or supersolid phases, as $S(\pi,\pi)$ is always non zero. There is no Mott phase and the superfluid phase is limited to the region where $\rho \lesssim 0.25$.

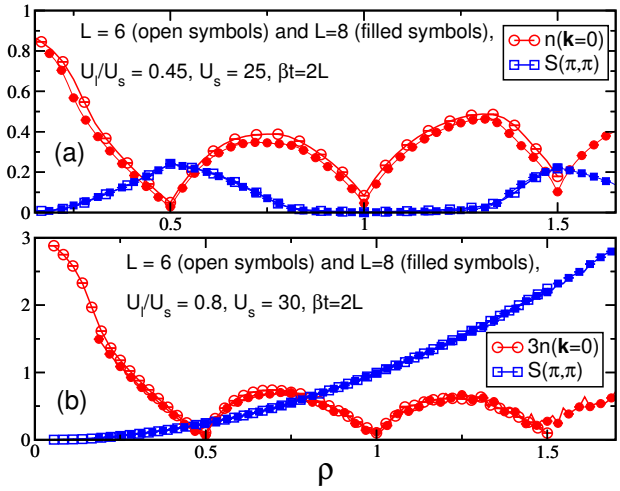


FIG. 7. (Color online) Cuts in the phase diagram as functions of $\rho$ for $U_l/U_s = 0.45$ (a) and $U_l/U_s = 0.8$ (b) and two different system sizes $L = 6$ and $L = 8$. In (a) we see the four phases SF, CDW, MI and SS (see text). In (b) we see that the larger value of $U_l$ forbids the existence of homogeneous phases except for low densities $\rho \lesssim 0.25$. On the contrary, we observe MI and SF phases in (a), i.e. regions where $S(\pi,\pi)$ is zero.

We remark that these results have been obtained at fixed densities (canonical ensemble). The stability of

these phases with regard to density fluctuations, i.e. the behaviour of the system in the grand canonical ensemble, will be discussed below (see Sec. IV C).

### B. Quantum Phase Transitions at fixed densities

We show here how the phase diagrams (Fig. 4) were obtained. To this end, we analyse the quantum phase transitions between the different phases, focusing on the $\rho = 1$ case, and using finite size scaling analysis. We summarize in Table. I the different types of phase transition that we observed. When a spatial modulation develops, as in the CDW or SS phases, the discrete $\mathbb{Z}_2$ translation symmetry is broken. When the superfluidity or condensate appears, the continuous $U(1)$ phase symmetry is broken. For the successive transitions between the superfluid, supersolid and CDW phases, these $\mathbb{Z}_2$ and $U(1)$ symmetries are then broken separately or simultaneously. When they are broken together, we expect a first order transition. When they are broken separately, we expect 3D Ising and 3D XY universality classes and our QMC results confirm this. We rescaled $n(\mathbf{k} = 0)$ by $L^{2\beta_{XY}/\nu_{XY}}$ and $S(\pi, \pi)$ by $L^{2\beta_{\rm Ising}/\nu_{\rm Ising}}$. $\beta_{XY}$ and $\nu_{XY}$ here denote the critical exponents of the 3D XY model and $\beta_{\rm Ising}$ and $\nu_{\rm Ising}$ those of the 3D Ising model. With this rescaling, we expect the curves obtained for different sizes to cross at a single point corresponding to the transition. Increasing $U_s/t$ for a given value of $U_l/U_s$, we observe such crossings for the SF-SS transition where $S(\pi, \pi)$ becomes non zero and for the SS-CDW transition where $n(\mathbf{k} = 0)$ becomes zero (see Fig. 8). We do not obtain such crossings if we use mean field scaling exponents.

The transitions between different solid phases are found to be of first order, as suggested by[12] for $\rho = 1$. To confirm this, we did QMC simulations with different starting states (CDW or MI), for a large enough system. In the region where both the MI and CDW (2,0) phases coexist, the system remains in the local energy minima corresponding to the phase with which we started the simulation. An hysteresis effect is then observed for $S(\pi, \pi)$ as $U_l/U_s$ is varied (Fig. 9(a)). In the coexistence region around the transition we obtain two different values of $S(\pi, \pi)$ while the two initial conditions yield the same values when we are far away from the transition point and no longer have coexistence of metastable and stable states.

| Quantum Phase Transitions | symmetry broken | Type |
|---|---|---|
| MI-SF | $U(1)$ | 3D XY |
| SS-CDW | $U(1)$ | 3D XY |
| SF-SS | $\mathbb{Z}_2$ | 3D Ising |
| MI-CDW | $\mathbb{Z}_2$ | first-order |
| SF-CDW (2,0) | $U(1), \mathbb{Z}_2$ | first-order |
| CDW (2,1)-CDW (3,0) | $\emptyset$ | first-order |

TABLE I. Universality classes for the quantum phase transitions of the phase diagrams Fig. 4, determined using quantum Monte Carlo simulations.

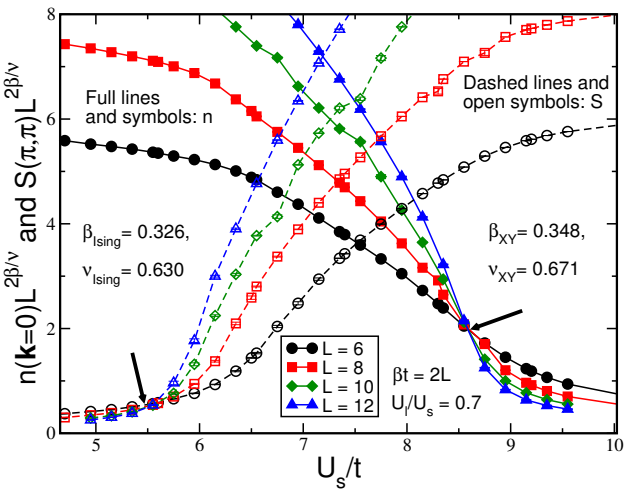


FIG. 8. (Color online) The transitions between the SF and SS and between the SS and the CDW phases for $\rho = 1$. The first transition is signalled by $S(\pi, \pi)$ becoming non zero (open symbols, dashed lines), while the second transition corresponds to $n(\mathbf{k} = 0)$ becoming zero (full symbols, full lines). In the intermediate supersolid region, both are non zero. The data have been rescaled with critical exponents $\beta_{\rm Ising}, \nu_{\rm Ising}$ for $S(\pi, \pi)$ and $\beta_{\rm XY}, \nu_{\rm XY}$ for $n(\mathbf{k} = 0)$, corresponding to different universality classes (3D XY and 3D Ising). The arrows point to the two transition points where the curves obtained for different sizes cross each other.

Examining the ground state energy, i.e. the free energy, measured with both initial states, the transition point is located where the two energy curves cross. Below this crossing point, the CDW state is metastable and the Mott state is stable (Fig. 9(b)), while the opposite is true above this point.

We observe the same hysteresis effects at $\rho = 1$ in the small region ($13 < U_s/t < 17$ in Fig. 4) between the SF and CDW phases. This confirms the presence of a direct first order transition from the SF to the CDW (2,0) in this region and the absence of a supersolid which then only exists for $U_s/t < 13$.

As the interaction $U_s/t$ grows, for $\rho = 1/2$ and $\rho = 3/2$, the PS and SS regions becomes narrower and eventually disappears. There is then a direct transition between SF and CDW (1,0) at $\rho = 1/2$ and between SF and CDW (2,1) at $\rho = 3/2$. We were not able to obtain a definite conclusion concerning the nature of these transitions, due to the difficulty of the QMC simulations in this large interaction regime.

For $\rho = 3/2$, we also observe a first order transition between the CDW (2,1) and the CDW (3,0) phases. This is somewhat surprising since the same spatial symmetry is broken in both phases and one might have expected a crossover. The proximity of this first order transition to

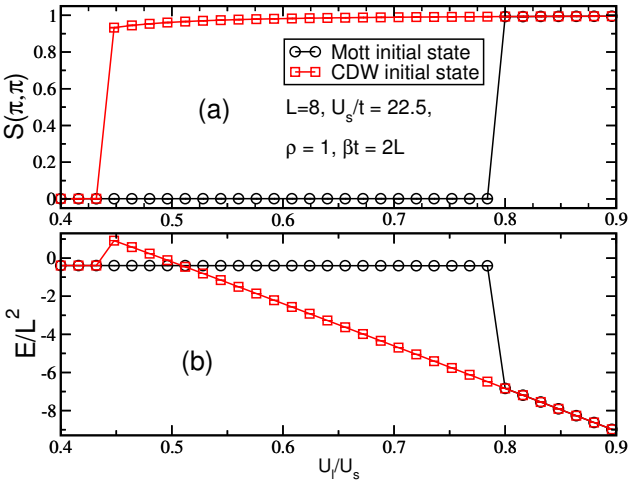


FIG. 9. (Color online) The structure factor (a) and ground state energy (b) obtained by varying $U_l/U_s$ around the MI-CDW(2,0) transition. The two curves in each panel correspond to different starting states for the QMC simulation that yield different results in the region where both phases coexist and the same result outside the coexistence region. The transition point is located at the point where the two ground state energy curves meet.

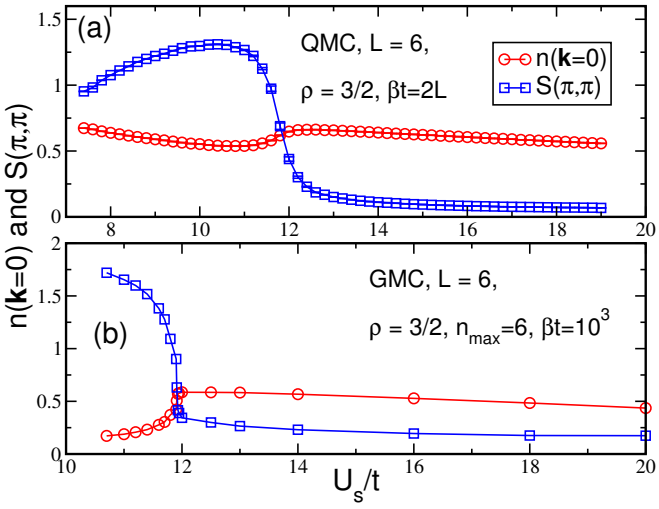


FIG. 10. (Color online) Cuts along lines inside the $\rho = 3/2$ supersolid phase (see the green lines in Figs. 3(c) and 4(c)) made with QMC (a) and GMC (b). In both cases, we observe a crossover between two different regimes. As $U_s/t$ grows ($U_l/U_s$ diminishes) the SS goes from a regime where $S(\pi,\pi)$ is large, due to the proximity with the CDW (3,0) phase, to a regime where it is much smaller, when the SS is close to the CDW (2,1). As the crossover between these two SS regimes happens (around $U_s/t = 12$), the condensate fraction $n(\mathbf{k}=0)$ increases.

the narrowing of the $\rho = 3/2$ SS phase (see Fig. 4(c)) raises the question of a possible transition between two different SS phases. Cutting along a line through the SS phase (see Fig. 4(c)), we do not find a transition but a crossover between two different regimes (Fig. 10(a)). Close to the CDW (3,0) phase ($U_s/t < 12$), the oscillations of density are much larger in the SS phase, which is marked by larger value of $S(\pi,\pi)$. $S(\pi,\pi)$ becomes much smaller close to the CDW (2,1) phase ($U_s/t > 12$). Such a large change is expected as, in the large interaction limit, $S(\pi,\pi)$ goes from 9/4 down to 1/4 between the CDW (3,0) and (2,1) phases. While $n(\mathbf{k}=0)$ generally decreases with increasing $U_s/t$, it increases slightly in the crossover region ($U_s/t \simeq 12$). We also observe this behaviour with the GMC approach (Fig. 10(b)).

### C. Stability of phases

So far, we mainly discussed the phases and transitions that appear at a constant particle number and mentioned that, in some cases, Hubbard systems can be unstable to phase separation as the density is allowed to fluctuate. In particular, it was shown that such a phase separation can occur between superfluid and solid phases and be mistaken for a stable supersolid phase[29]. This is especially important in the present case as long range attractive interactions, if strong enough, tend to destabilize the system and lead to a collapse of the particles (for example for $U_l/U_s > 1$ in the MF description) or to the presence of metastable states[30].

We, therefore, analyse the stability of phases by studying the evolution of the density, $\rho$, as a function of the chemical potential $\mu$. In the grand canonical ensemble $\rho$ is calculated directly as an average for a given value of $\mu$. In the canonical ensemble, $\rho$ is fixed and $\mu$ can be calculated, for $kT \simeq 0$, as $\mu(N) = E(N+1) - E(N)$ where $E(N)$ is the ground state energy of the system with $N$ particles. In the GCE, an unstable region is characterized by a jump in the density as $\mu$ is varied. The intermediate densities do not correspond to a stable phase. Using CE, one can choose a filling corresponding to these intermediate densities but then the region is signalled by a curve $\rho(\mu)$ with a negative slope[29].

We found that some regions of the phase diagrams are unstable. For example doping around $\rho = 0.5$ for $U_s/t = 5.5$ and $U_l/U_s = 1$ (Fig. 11(a)), we observe a large unstable region which encompasses $\rho = 0.5$ and leads directly from a superfluid phase for $\rho \lesssim 0.39$ to a supersolid phase for $\rho \gtrsim 0.60$. This is attested by the behavior of $\rho(\mu)$: a jump is observed in the GCE simulations and a corresponding negative slope region is observed in CE simulations. This means that what appears to be a supersolid phase with the canonical simulations for $\rho = 0.5$ in the phase diagram Fig. 4(a) is, as mentioned earlier, not a stable phase but corresponds to a region of separation between SF and SS phases (SF-SS PS region in Fig. 4(a)).

On the other hand, cutting through the phase diagram at $U_s/t = 6.5$ and $U_l/U_s = 0.8$ (Fig. 11(b)), i.e. going through the SS regions at $\rho = 1$ and $\rho = 1.5$ (see Fig.

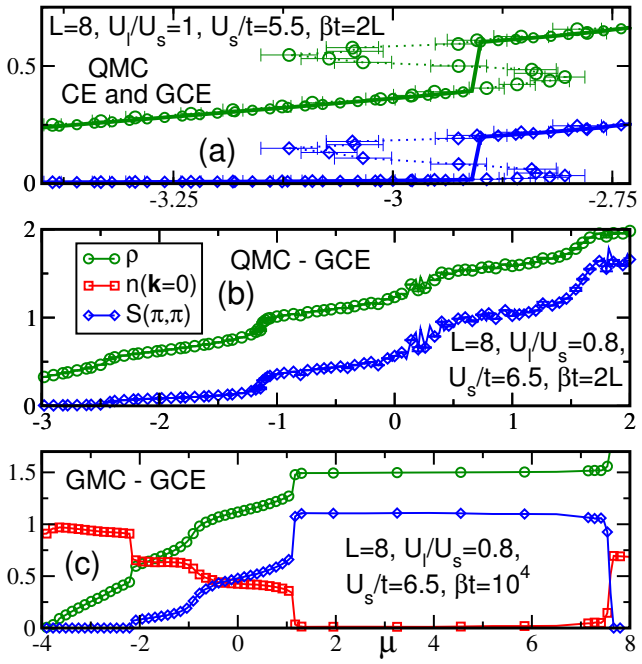


FIG. 11. (Color online) $\rho$, $n(\mathbf{k}=0)$ and $S(\pi,\pi)$ vs $\mu$. Dotted lines correspond to canonical simulations while continuous lines correspond to grand canonical ones. (a) Using QMC CE simulations, we observe a region in $\rho(\mu)$ with negative slope around $\rho = 1/2$ indicating instability. $n(\mathbf{k}=0)$ is always non zero (not shown to keep the figure uncluttered). There is, therefore, a discontinuous transition from a superfluid for $\rho \lesssim 0.39$ to a supersolid for $\rho \gtrsim 0.60$ which is also signalled by a jump in $\rho(\mu)$ when using the GCE. There is no stable phase at $\rho = 0.5$ for these parameters. (b) For a different set of parameters, we do not observe jumps in the $\rho(\mu)$ curve (QMC GCE simulations) which shows that the supersolid phases at $\rho = 1$ and $\rho = 1.5$ are stable. $n(\mathbf{k}=0)$ is always non zero (not shown). (c) Similar behavior is observed using the Gutzwiller approximation. In the case presented here we observe a direct transition from SF at $\rho \lesssim 0.44$ to SS for $\rho \gtrsim 0.58$ and a discontinuous transition from SS for $\rho \lesssim 1.29$ to solid phase for $\rho = 1.5$. We then have two density regions where the system is unstable. In (b) and (c) $S(\pi,\pi)$ has been multiplied by 0.5 to improve visibility.

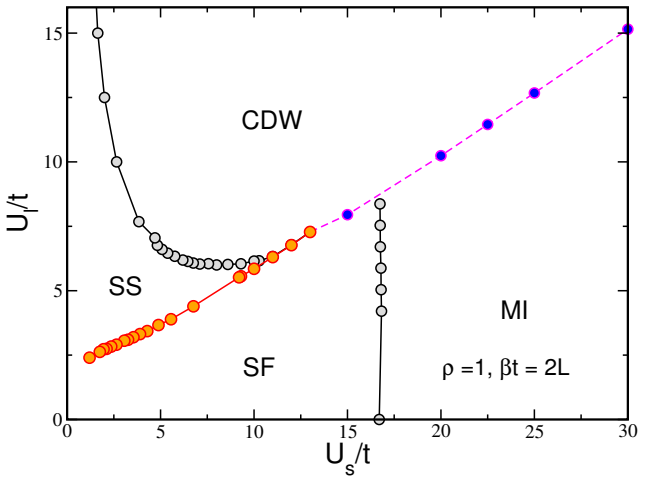


FIG. 12. (Color online) The phase diagram (Fig. 4 (b)) for $\rho = 1$ rescaled for a direct comparison with experimental data (figure 2 of extended data[12]). Compared to the experiment, the superfluid and supersolid regions are found to be smaller.

4(b) and (c)), we do not observe jumps in $\rho(\mu)$ using GCE simulation (Fig. 11(b)) and conclude that the supersolid phases are in fact stable for these densities, with these parameters. Finally, we performed some simulations (not shown here) for large values of the interactions ($U_s/t = 30, U_l/U_s = 0.8$) where we observed that the only stable phases are the solid phases obtained for integer or half-integer densities: there is no stable superfluid or supersolid phases for intermediate densities.

This question of stability can also be addressed within the Gutzwiller approximation. In Fig. 11(c), we observe jumps in $\rho(\mu)$ that mark the presence of unstable regions. In particular, again observe that the system is not stable for $\rho = 0.5$ and that there is a SF-SS discontinuous transition around that density. The parameters used for Fig. 11(b) and (c) are the same but, as the phase diagrams Fig. 3 and Fig. 4 are slightly different, the phases that are present in these two cuts are different. For example, at $\rho = 1.5$, we find a SS phase in the QMC simulations while we have a solid phase in the GMC simulations.

## V. CONCLUSIONS

Using exact quantum Monte Carlo and approximate mean field calculations, we studied the phase diagram of a bosonic Hubbard model with infinite range interactions which has been proposed to describe recent experimental results of the ETH-Zurich group[12]. Our results confirm that the model correctly captures the essential physics of the experiments. In particular, we confirm the existence of a supersolid phase and also the nature of the phase transitions, especially the first order transition between the MI and CDW at $\rho = 1$. We observe a small region where there is, at $\rho = 1$, a direct first order SF to CDW transition that was not experimentally observed.

There remains, however, quantitative differences in the extent of the different phases. This is easier to discuss by comparing the phase diagram Fig. 12, represented in the plane $(U_s/t, U_l/t)$, with the one provided as Figure 2 of extended data in Ref. 12. In the experimental data, the SF phase is observed up to $U_s/t \simeq 25$ whereas we observe a transition around $U_s/t \simeq 17$. The SS region is also much larger in the experimental figure extending up to $U_s/t \simeq 30$ and $U_l/t \simeq 25$ whereas we observe it in the region where $U_s/t$ and $U_l/t$ are smaller than 10. We believe these discrepancies to be due to the fact that we performed bulk simulations (i.e. with no trap) whereas

the experiment takes place in a harmonic trap. However, the main point is that the existence of the supersolid phase observed in the experiment is confirmed. It is a true thermodynamically stable phase and not a simple mixture of superfluid and solid phases.

We also extended the phase diagram to other densities and confirmed predictions that were made using mean-field calculations[17,18]. We also discussed the stability of the observed phases with respect to phase separation and found that the $\rho = 1$ and $\rho = 1.5$ supersolid phases are stable whereas there is phase separation between a SF and a SS for $\rho = 1/2$.

## ACKNOWLEDGMENTS

We thank T. Roscilde for constructive discussion on the GMC technique. We thank G. Morigi and T. Donner for useful discussions. This work is supported by the Alexander von Humboldt-Foundation. Some calculations have been performed on the PSMN centre of the ENS-Lyon.

* Corresponding author: frederic.hebert@unice.fr

[1] I. Bloch, J. Dalibard, and W. Zwerger, Rev. Mod. Phys. **80**, 885 (2008).
[2] M. Greiner, O. Mandel, T. Esslinger, T.W. Hänsch, and I. Bloch, Nature **415**, 39 (2002).
[3] Cheng Chin, R. Grimm, P. Julienne, and E. Tiesinga, Rev. Mod. Phys. **82**, 1225 (2010).
[4] H. Ritsch, P. Domokos, F. Brennecke, and T. Esslinger, Rev. Mod. Phys. **85**, 553 (2013).
[5] K. Baumann, C. Guerlin, F. Brennecke, T. Esslinger, Nature **464**, 1301 (2010).
[6] J. Klinder, H. Keßler, M.R. Bakhtiari, M. Thorwart, and A. Hemmerich, Phys. Rev. Lett. **115**, 230403 (2015).
[7] G. Labeyrie, E. Tesio, P. M. Gomes, G.-L. Oppo, W. J. Firth, G. R. M. Robb, A. S. Arnold, R. Kaiser, T. Ackemann, Nature Photon. **8**, 321 (2014).
[8] S. Ostermann, F. Piazza, and H. Ritsch, Phys. Rev. X **6**, 021026 (2016).
[9] H. Habibian, A. Winter, S. Paganelli, H. Rieger, and G. Morigi, Phys. Rev. Lett. **110**, 075304 (2013).
[10] K. Rojan, R. Kraus, T. Fogarty, H. Habibian, A. Minguzzi, and G. Morigi, Phys. Rev. A **94**, 013839 (2016).
[11] B. Zhu, J. Schachenmayer, M. Xu, F. Herrera, J.G. Restrepo, M.J. Holland, and A.M. Rey, New Journal of Physics **17**, 083063 (2015).
[12] R. Landig, L. Hruby, N. Dogra, M. Landini, R. Mottl, T. Donner, and T. Esslinger, Nature **532**, 476 (2016).
[13] O. Penrose and L. Onsager, Phys. Rev. **104**, 576 (1956).
[14] E.P. Gross, Phys. Rev. B **106**, 161 (1957).
[15] J. Léonard, A. Morales, P. Zupancic, T. Esslinger, and T. Donner, arXiv:1609.09053 [cond-mat.quant-gas]
[16] M. R. Bakhtiari, A. Hemmerich, H. Ritsch, and M. Thorwart, Phys. Rev. Lett. **114**, 123601 (2015).
[17] N. Dogra, F. Brennecke, S.D. Huber, and T. Donner, Phys. Rev. A **94**, 023632 (2016).
[18] B. Sundar and E. J. Mueller, Phys. Rev. A **94**, 033631 (2016).
[19] Y. Chen, Z. Yu, and H. Zhai, Phys. Rev. A **93**, 041601 (2016).
[20] J. Panas, A. Kauch, and K. Byczuk, arXiv:1607.00671
[21] A. E. Niederle, G. Morigi, and H. Rieger, Phys. Rev. A **94**, 033607 (2016).
[22] C. Hickey and A. Paramekanti, Phys. Rev. Lett. **113**, 265302 (2014).
[23] T. Roscilde, private communication.
[24] N. Metropolis, A. W. Rosenbluth, M. N. Rosenbluth, A. H. Teller, and E. Teller, Journal of Chemical Physics **21**, 1087 (1953).
[25] V.G. Rousseau, Phys. Rev. E **77**, 056705 (2008).
[26] V.G. Rousseau, Phys. Rev. E **78**, 056707 (2008).
[27] D.M. Ceperley and E.L. Pollock, Phys. Rev. **B39**, 2084 (1989).
[28] T. Ohgoe, T. Suzuki, and N. Kawashima, Phys. Rev. B **86**, 054520 (2012).
[29] G.G. Batrouni and R.T. Scalettar, Phys. Rev. Lett. **84**, 1599 (2000).
[30] C. Menotti, C. Trefzger, and M. Lewenstein, Phys. Rev. Lett. **98**, 235301 (2007).